Supporting Information

Low-valent cation substitution engineering regulates Li_2S durable electrodeposition in practical lithium-sulfur batteries

Jiyang Tian [a], Jiajun Wan [a], Qian Zhang [b, *], Huibo Zhang [a], Jie Liu [a, *]

[a] *Youth Innovation Team of Shandong Higher Education Institutions, College of Chemical Engineering, Qingdao University of Science and Technology, Qingdao 266042, Shandong, P. R. China*

[b] *Weifang Key Laboratory of Green Processing of Separator for Chemical Power Sources, School of Chemistry and Engineering, Weifang Vocational College, Weifang, Shandong 261108, P. R. China*

[*] Corresponding Authors.

E-mail address: jie.liu@qust.edu.cn (Jie Liu); 2021010014@sdwfvc.edu.cn (Qian Zhang)

Methods

Synthesis of $LaCu_{0.5}Co_{0.5}O_{3-x}$ (LCCO)

The LCCO was synthesized via a sol-gel technique. 2 mM $Co(NO_3)_2 \cdot 6H_2O$ (AR, Sinopharm Chemical Reagent Co., Ltd.), 2 mM $Cu(NO_3)_2 \cdot 3H_2O$ (AR, Aladdin), and 4 mM $La(NO_3)_3 \cdot 6H_2O$ (AR, Aladdin) were dissolved in 50 mL of deionized (DI) water, followed by the addition of 12 mM polyvinylpyrrolidone (PVP, AR) under continuous stirring for 30 min (solution I). 12 mM citric acid was dissolved in 30 mL of DI water (solution II) and subsequently introduced into solution I. The resulting solution was stirred at 60 °C until gelation. The gel precursor was dried in air at 100 °C for 12 h, and then calcined at 800 °C

under air for 4 h, yielding the LCCO.

Characterization

The crystal phase of the sample was studied by X-ray diffraction spectroscopy (XRD, Bruker D8 Advance). The morphology diagrams of the materials were obtained by scanning electron microscopy (SEM, JEOL JSM-7800F) and transmission electron microscopy (TEM, JEOL JEM-2800). The surface electronic states and compositional evolution of LCCO before and after polysulfide adsorption were examined by X-ray photoelectron spectroscopy (XPS, Thermo Scientific ESCALAB 250Xi). In-situ Raman spectra were recorded on a Raman spectroscopy (Renishaw, invia Qontor).

Electrochemical tests

For composite separator preparation, LCCO, Super P, and polyvinylidene fluoride (PVDF, battery grade) binder at a mass ratio of 6:3:1 were mixed, using N-methyl-2-pyrrolidone (NMP, AR, Aladdin) solvent. Then the obtained slurry was uniformly coated onto one side of commercial Celgard 2325 separators and vacuum-dried at 60 °C for 12 h.

To prepare S/Super P composite, sulfur powders (AR, Aladdin) and Super P (battery grade, Aladdin) were blended at a mass ratio of 6:4 or 8:2, sealed in a Teflon-lined autoclave, and thermally treated at 155 °C for 12 h. The obtained S/Super P composite was then mixed with Ketjen black (KB, AR) and guar gum (5000-5500 cps, Aladdin) binder (8:1:1, by mass) in DI water to form a uniform slurry. The obtained slurry was cast onto carbon-coated Al foil and vacuum-dried at 60 °C for 12 h to achieve the sulfur cathodes. The high-loading sulfur cathodes were coated on carbon paper.

CR2016 coin cells were assembled using the sulfur cathode, LCCO-modified separator,

and lithium anode in the glove box. The electrolyte consisted of 1 M lithium bis(trifluoromethanesulfonyl)imide (LiTFSI) with 2 wt% $LiNO_3$ in a 1:1 (v/v) mixture of 1,3-dioxolane (DOL) and 1,2-dimethoxyethane (DME). Galvanostatic charge-discharge tests were conducted at 25 °C on a LAND CT3002A battery testing system. Cyclic voltammetry (CV) was carried out on a Corrtest CS2350M electrochemical workstation in the potential range of 1.8-2.6 V at 0.1 - 0.5 mV s^{-1}. Electrochemical impedance spectroscopy (EIS) was performed over 10 mHz-100 kHz with a 5 mV perturbation. For the GITT test, a constant current of 0.1 C was used for discharge (or charge) of 10 min, followed by a standing of 60 min.

Polysulfide adsorption and blocking

A Li_2S_6 solution (0.1 mol L^{-1}) was prepared by dissolving Li_2S (AR, Aladdin) and sulfur powders at a molar ratio of 1:5 in 6 mL of DOL/DME (1:1 v/v) under stirring at 65°C for 48 h. The solution was subsequently diluted to 2 mmol L^{-1} for polysulfide adsorption tests. 0.16 g of LCCO, LCO, and LO powders were added to separate glass vials containing equal volumes of the Li_2S_6 solution. After standing for 48 h, the supernatants were collected for spectroscopic analysis. Ultraviolet-visible (UV-vis) absorption spectroscopy (Metash UV-8000) was employed to quantify the residual Li_2S_6 after polysulfide adsorption.

For polysulfide diffusion experiments, a H-type glass cell was assembled with 35 mL of Li_2S_6 solution in the left chamber and an equal volume of DOL/DME (1:1 v/v) in the right chamber. The two compartments were separated by different membranes: polypropylene (PP) and LCCO-coated separators. The time-dependent color changes in the right chamber were monitored to analyze the polysulfide blocking capability.

Polysulfide catalytic performance

The activation energy could be calculated based on the Tafel slope according to equation (1)：

$$E_a = E_a^0 + \alpha nF\Delta\varphi_{cathode}, E_a = E_a^0 - \beta nF\Delta\varphi_{anode} \quad (1)$$

where E_a is the activation energy of the reaction process, E_a^0 is the intrinsic activation energy, α and β are the symmetry coefficient, n is the number of charge transfer, F is the Faraday's constant, $\Delta\varphi$ is the irreversible potential during cycling.

The Tafel slope can be calculated according to equation (2)-(4):

$$\eta = \frac{2.3RT}{\alpha nF}\log i_c^0 - \frac{2.3RT}{\alpha nF}\log i_c, \eta = -\frac{2.3RT}{\beta nF}\log i_a^0 + \frac{2.3RT}{\beta nF}\log i_a \quad (2)$$

$$\eta = a + b\log i \quad (3)$$

where η is the overpotential, i_c^0 and i_a^0 are the cathode and anode exchange current density, i_c and i_a are the current of the cathode and anode, a is the intercept of the Tafel curve, b is the slope of the Tafel curve.

$$b = -\frac{2.3RT}{\alpha nF}, b = \frac{2.3RT}{\beta nF} \quad (4)$$

Therefore, equation (1) can be written in a more concise form:

$$E_a = E_a^0 - \frac{2.3RT}{b}\Delta\varphi \quad (5)$$

Li_2S nucleation and dissolution

A Li_2S_8 solution (0.2 mol L^{-1}) was synthesized by dissolving Li_2S and sulfur powders at a molar ratio of 1:7 in the electrolyte under stirring at 65 °C for 48 h. For nucleation experiments, cathodes composed of carbon substrates loaded with LCCO, LCO, or LO were paired with lithium foil anodes and Celgard 2325 separators. Each cell was injected with 30 μL of Li_2S_8 solution on the cathode side and 30 μL of electrolyte on the anode side. Galvanostatic discharge

was conducted at 0.112 mA until the potential reached 2.06 V, followed by a potentiostatic discharge at 2.04 V until the current was < 10^{-3} mA.

The Li_2S nucleation and growth rate could be indicated according to equation (6):

$$Ak^2 = \frac{2}{\pi t_m^3} \quad (6)$$

where A stands for the nucleation rate (cm^{-2} s^{-1}), k is the growth rate (cm s^{-1}), and t_m stands for the peak time (s).

For Li_2S dissolution, cells were assembled using LCCO electrode, prepared by ultrasonically dispersing LCCO in ethanol and then dropping it onto carbon paper. A Li_2S_8 solution (0.2 mol L^{-1}) was used as the cathode electrolyte. Cells were first discharged to 1.7 V at 0.112 mA. Then the discharged cells were charged at a constant potential of 2.35 V until complete oxidation of solid Li_2S to soluble polysulfides.

Theoretical computations

Density functional theory (DFT) calculations were carried out to theoretically predict the adsorption-catalytic performance of the functional materials. The Perdew-Burke-Erzenhoff (PBE) form of the generalized gradient approximation (GGA) was employed to describe exchange and correlation effects. The GGA + U calculations were performed with U_{eff} (U_{eff} = Coulomb U - exchange J) values of 3.0 eV, 5.0 eV for Co and La, respectively. The cut-off energy was set as 500 eV, and the convergence criteria for self-consistent electronic energy and residual force were respectively assumed to be 10^{-5} eV/atom and 0.02 eV/Å, which could ensure sufficient accuracy. A slab of 156 atoms with O vacancies (V_O) is employed to model LCCO (121) surface. A vacuum region with a 35 Å vacuum layer was added between periodic slabs. A k-point mesh of 1 × 1 × 1 based on Monkhorst-Pack meshes was used for all structures. We

constructed a model where one Li_2S_6 molecule was adsorbed on the Co, La, and Cu sites of the LCCO (121) surface. The adsorption energy (E_{ads}) is expressed by the equation (7):

$$E_{ads} = E_{final} - E_{initial} - E_{Li_2S_6} \quad (7)$$

Where E_{final} and $E_{initial}$ refer to the energy after and before adsorption, respectively.

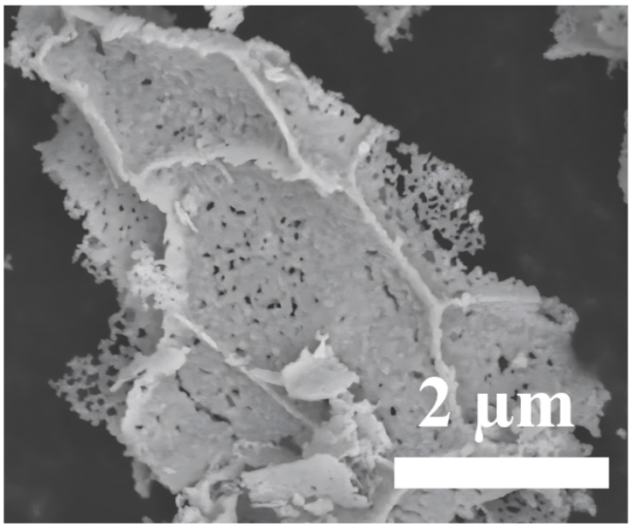

Fig. S1. SEM image of the as-prepared LCCO.

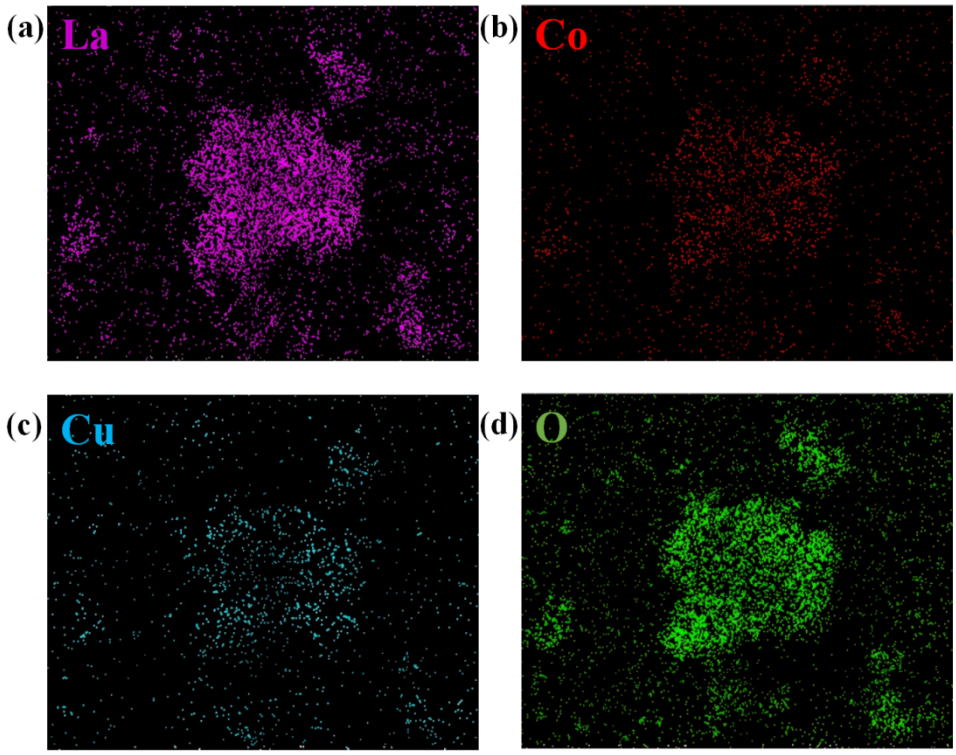

Fig. S2. Element mappings for (a) La, (b) Co, (c) Cu, and (d) O of the as-prepared LCCO.

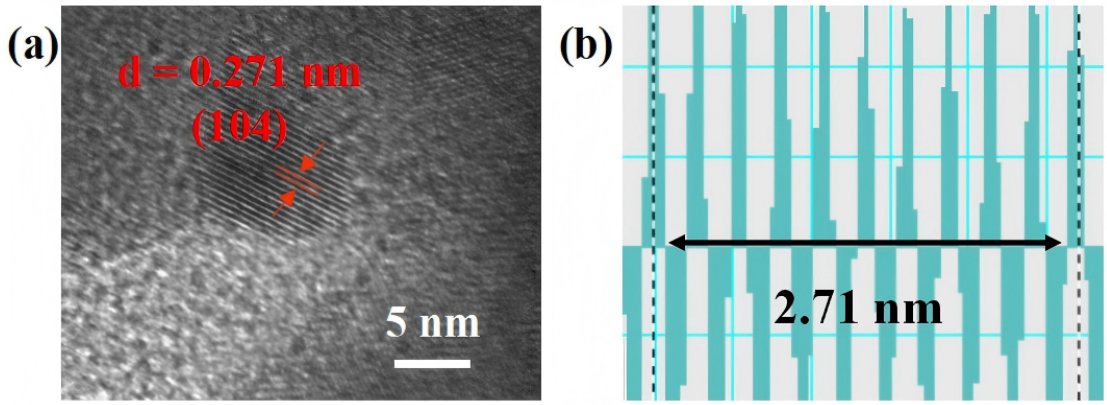

Fig. S3. (a) HRTEM image of the LCCO and (b) corresponding lattice spacing.

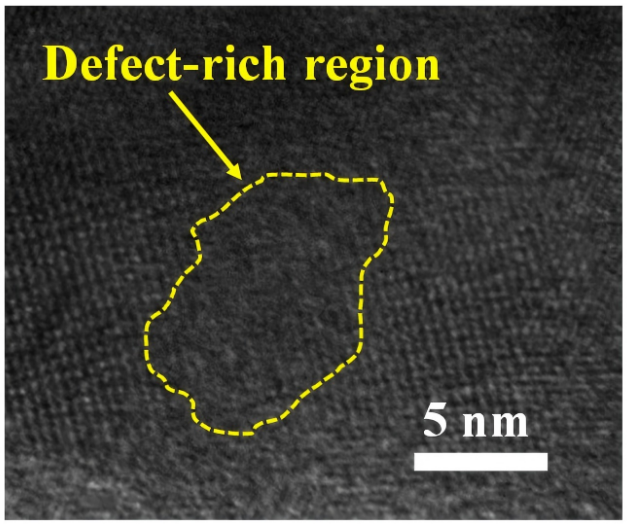

Fig. S4. TEM image of the LCCO with defect-rich region.

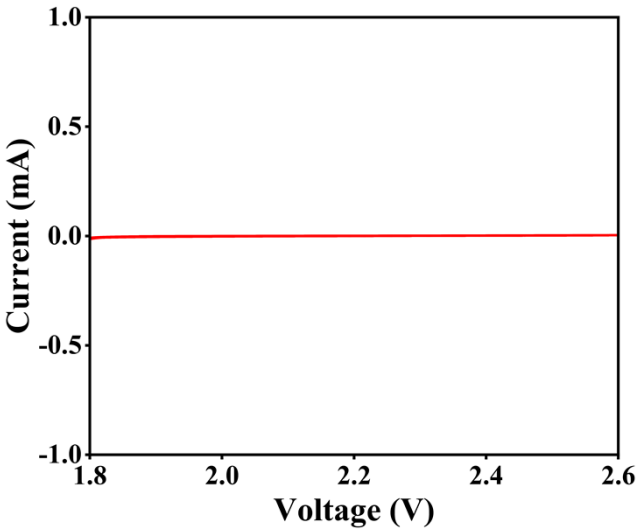

Fig. S5. The CV curve at 0.1 mV s^{-1} for the LCCO cathode without sulfur.

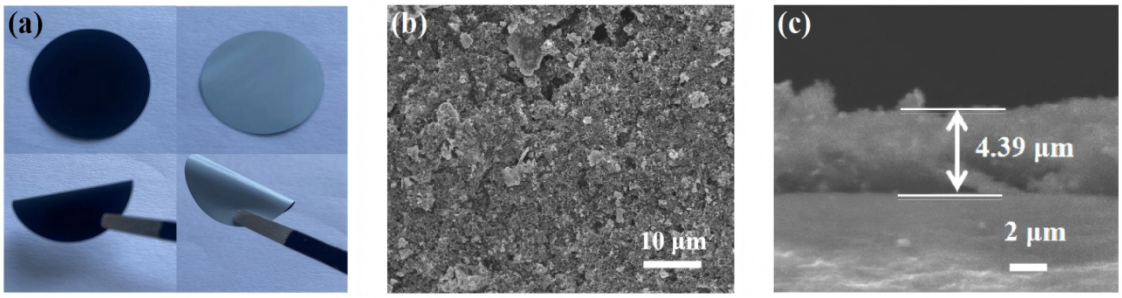

Fig. S6. (a) Digital photos of as-prepared LCCO-separator. (b) Top-view and (c) cross-section SEM images of LCCO-separator.

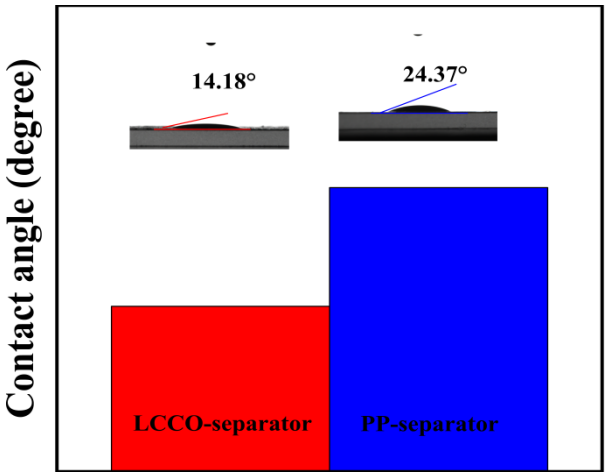

Fig. S7. Contact angle of LCCO-separator and PP-separator toward the electrolyte.

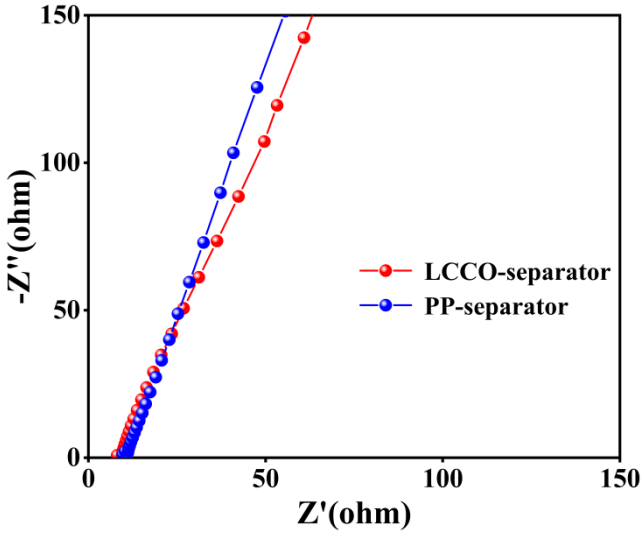

Fig. S8. Nyquist plots of occluded batteries using LCCO-separator and PP-separator.

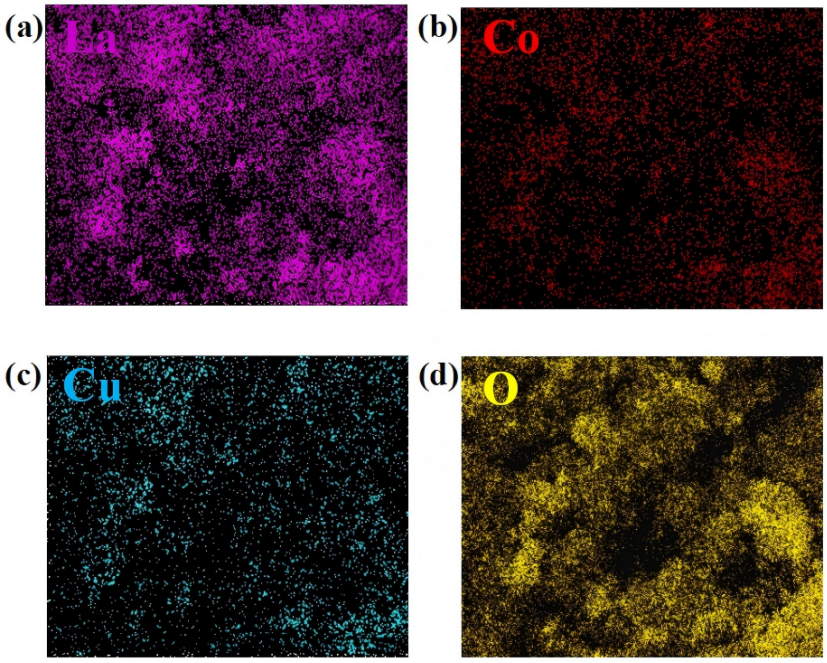

Fig. S9. Element mappings of the LCCO-separator.

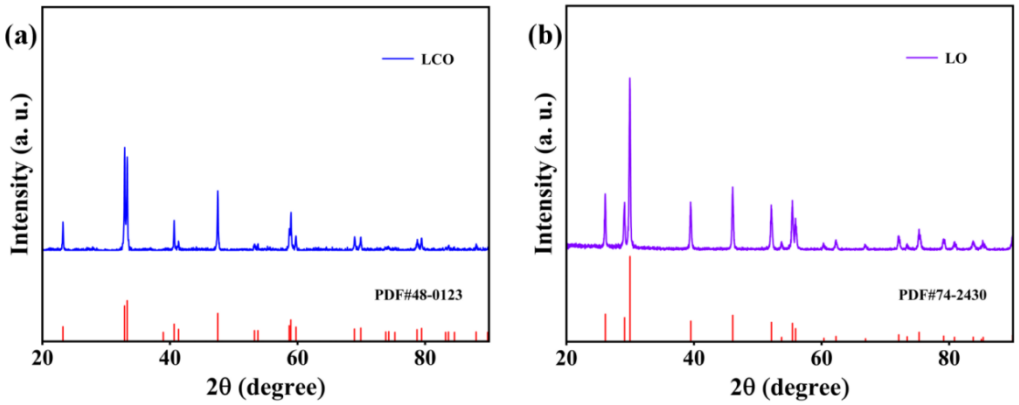

Fig. S10. XRD patterns of the (a) LCO and (b) LO.

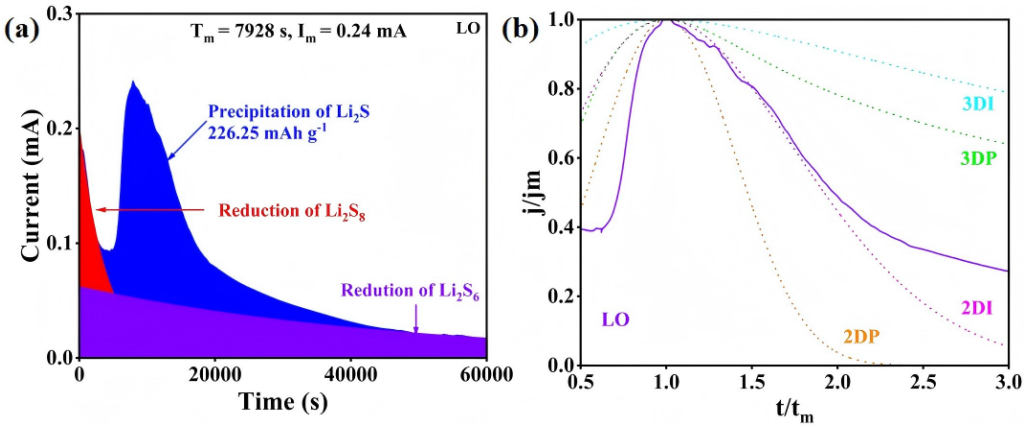

Fig. S11. (a) Li_2S nucleation curve on the LO electrode. (b) The theoretical and dimensionless transient models of Li_2S growth on the LO electrode.

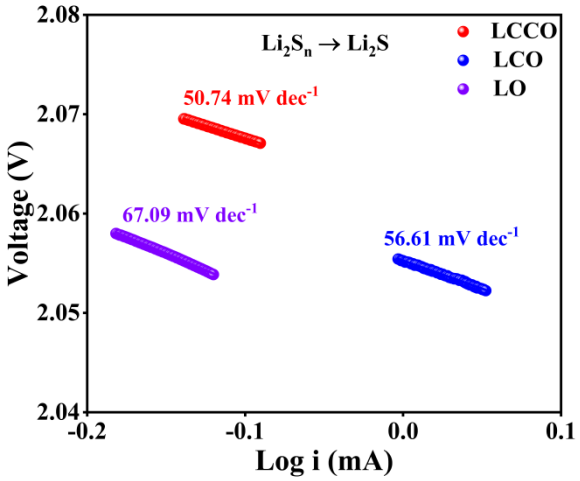

Fig. S12. Tafel slopes for the reduction of Li_2S_n to Li_2S.

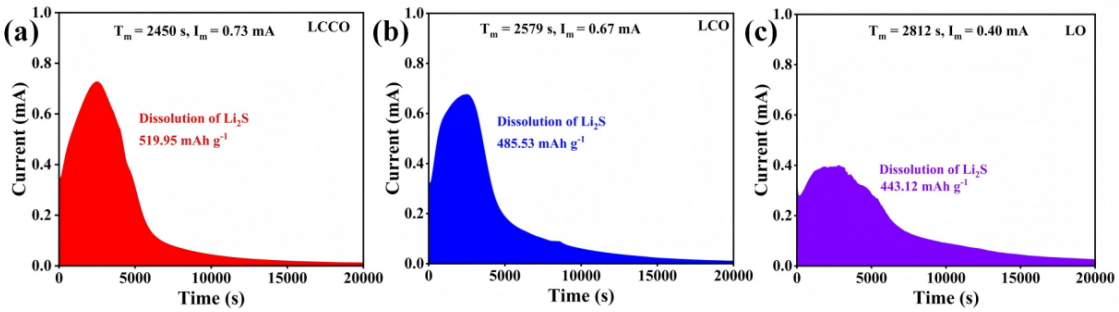

Fig. S13. Li_2S dissolution curves for (a) LCCO electrode, (b) LCO electrode, and (c) LO electrode.

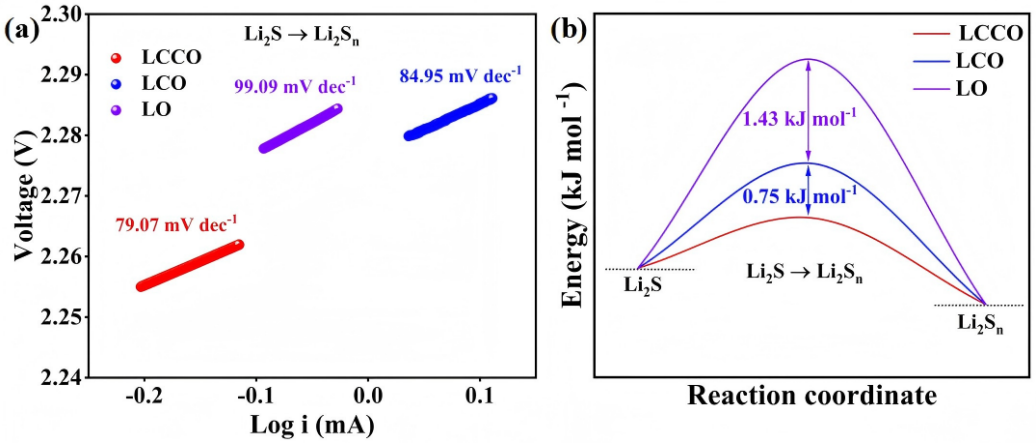

Fig. S14. (a) Tafel slopes and (b) relative activation energies for the oxidation of Li_2S to Li_2S_n.

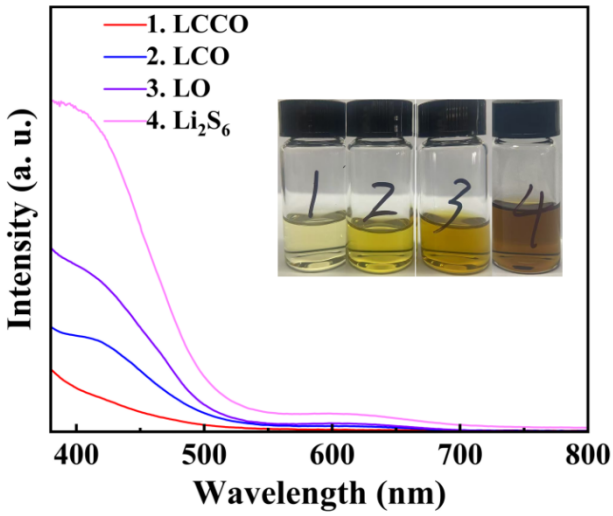

Fig. S15. UV-vis spectra of the Li_2S_6 solution after polysulfide adsorption tests (inset is the photo of the Li_2S_6 solutions after polysulfide adsorption tests).

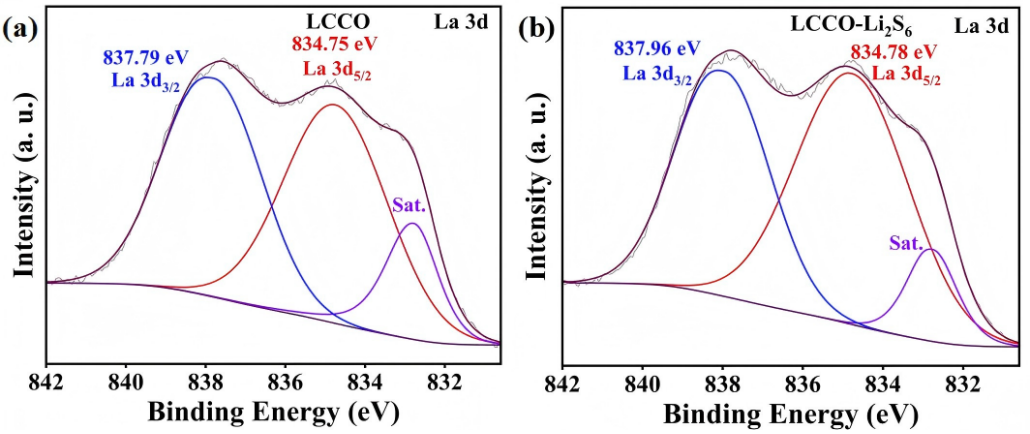

Fig. S16. (a, b) High-resolution XPS spectra of La 3d for LCCO before and after adsorbing Li_2S_6.

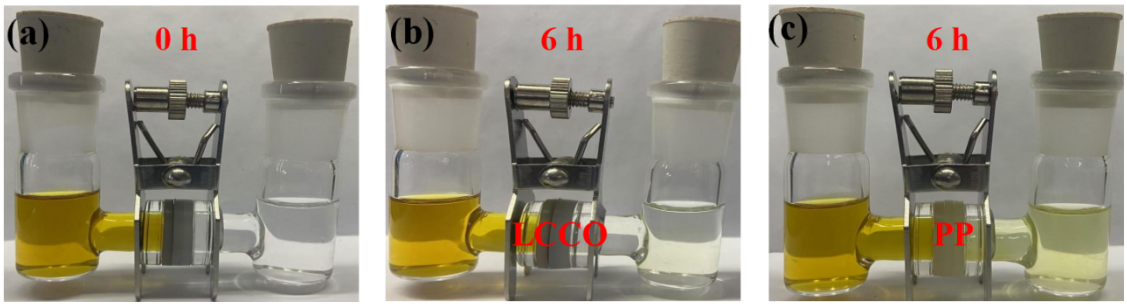

Fig. S17. (a-c) The photos of the polysulfide diffusion experiment using LCCO-separator and PP-separator.

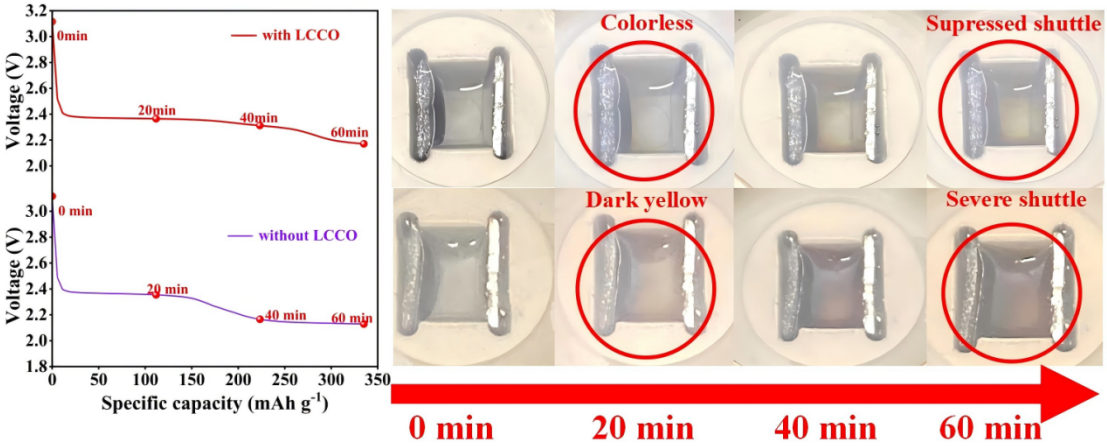

Fig. S18. Discharge curves and the digital photos of in-situ cells using the sulfur electrode with and without LCCO surface coating.

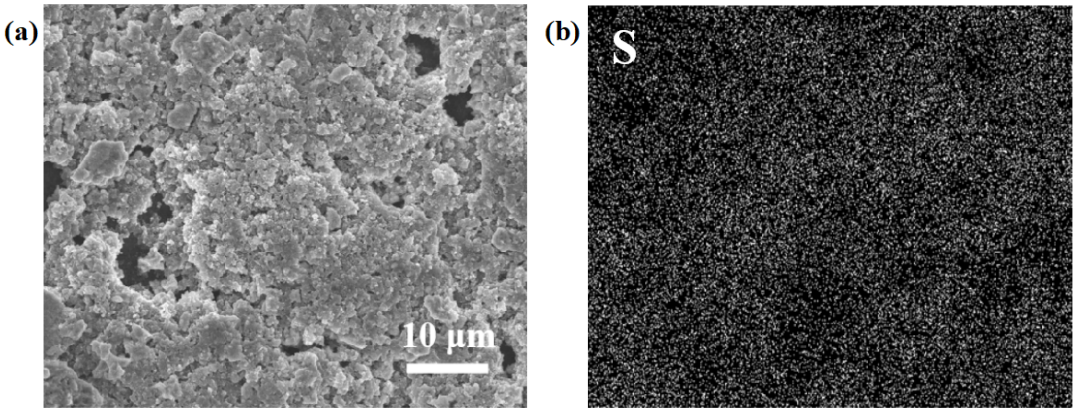

Fig. S19. (a) Top-view SEM image and (b) sulfur element mapping of the LCCO-separator after cycling.

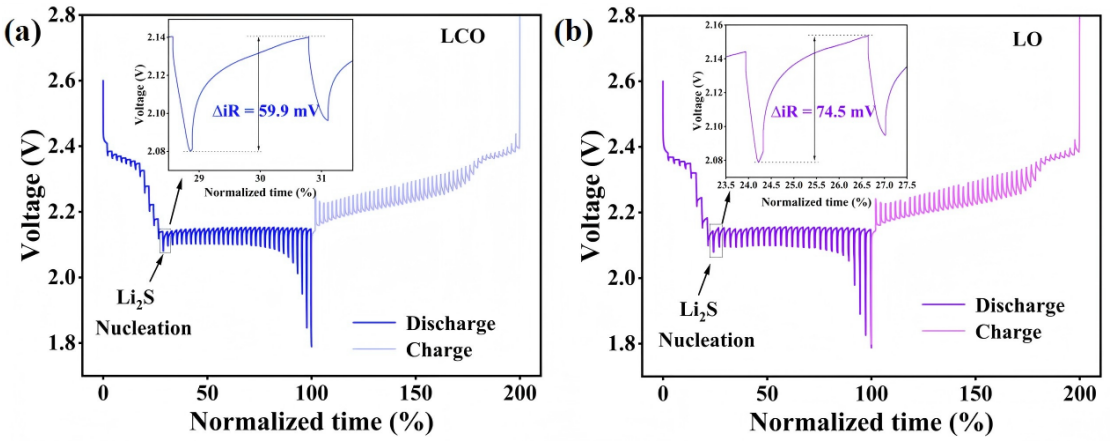

Fig. S20. GITT profiles of Li-S batteries with (a) LCO-separator and (b) LO-separator.

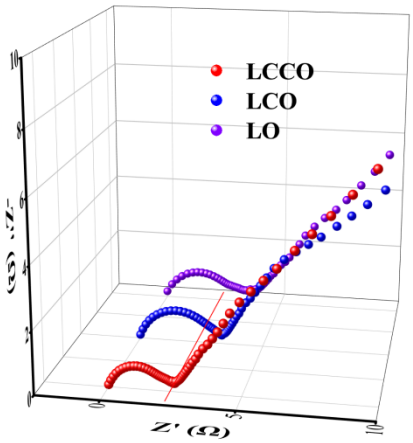

Fig. S21. Nyquist plots of the Li-S batteries after cycling with different separators.

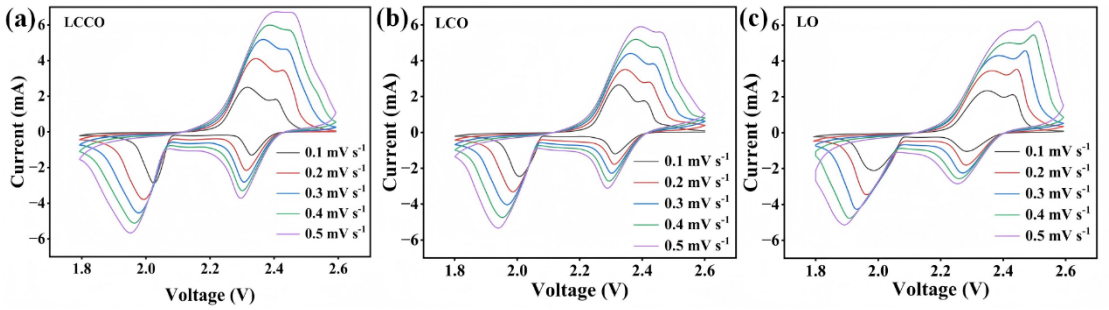

Fig. S22. CV curves for Li-S batteries with (a) LCCO-separator, (b) LCO-separator, and (c) LO-separator at different scan rates.

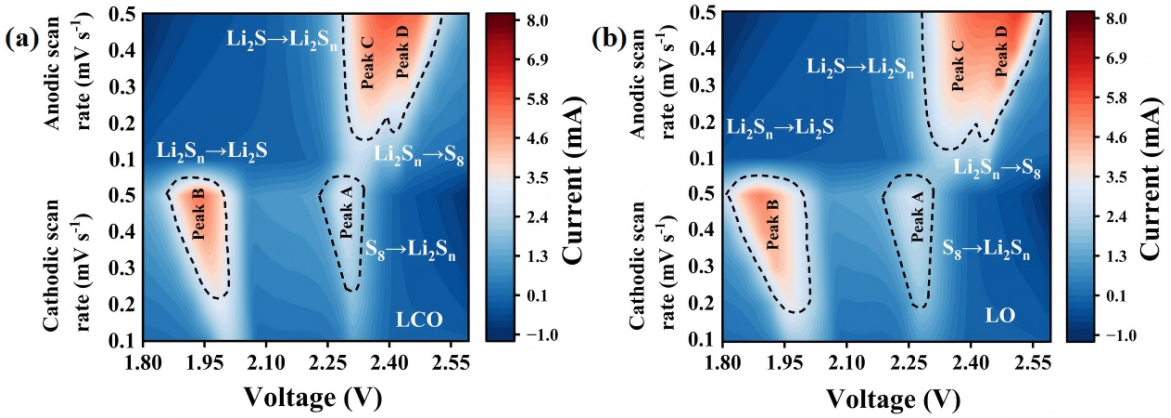

Fig. S23. Contour plots of CV curves for Li-S batteries with (a) LCO-separator and (b) LO-separator at different scan rates.

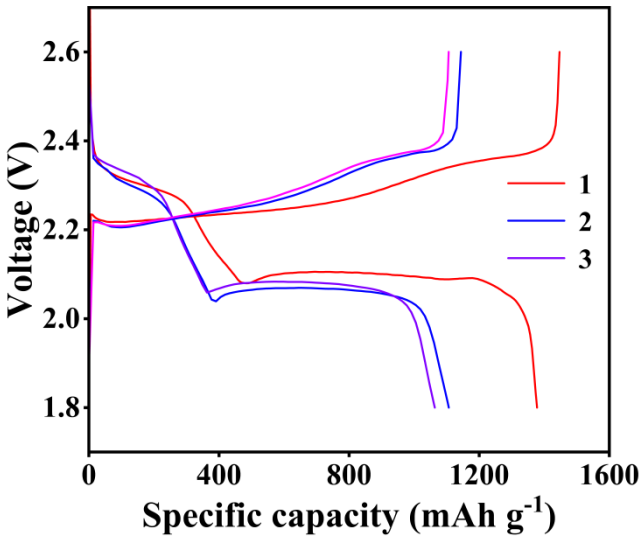

Fig. S24. Charge-discharge curves of Li-S batteries with LCCO-separator.

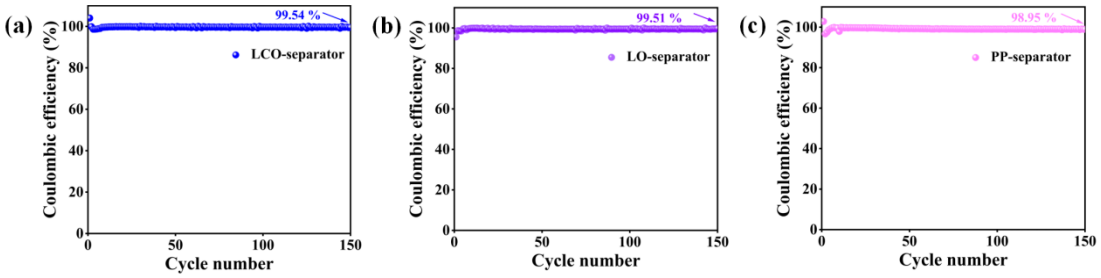

Fig. S25. Coulombic efficiency of the Li-S batteries with (a) LCO-separator, (b) LO-separator, and (c) PP-separator at 0.5 C.

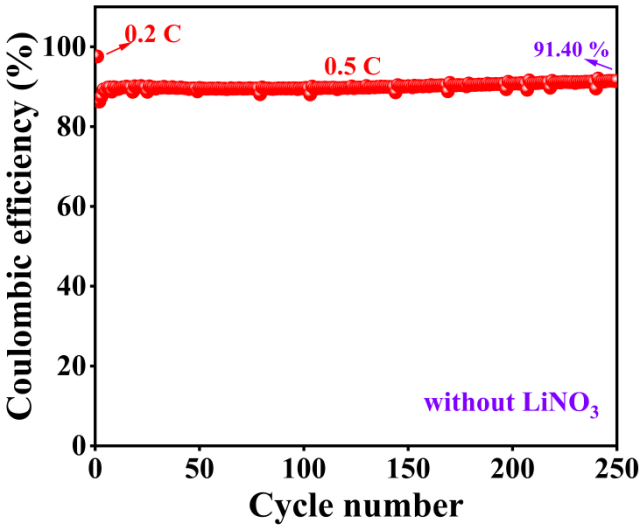

Fig. S26. Coulombic efficiency of Li-S battery using LCCO-separator in $LiNO_3$-free electrolyte.

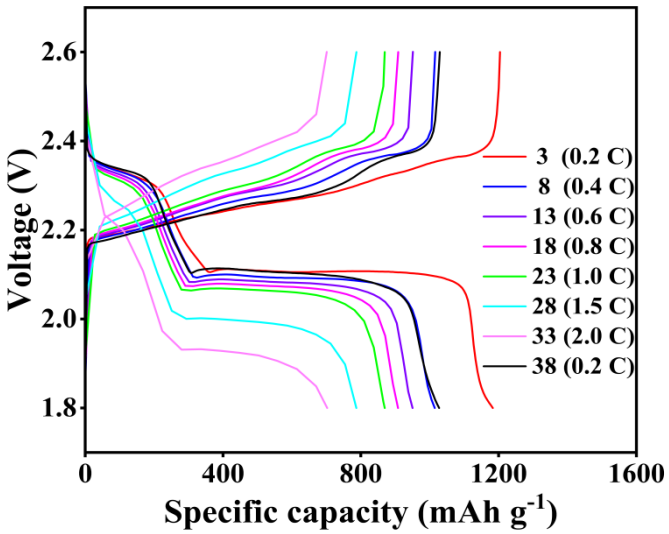

Fig. S27. The charge-discharge curves of the Li-S battery with LCCO-separator at different rates.

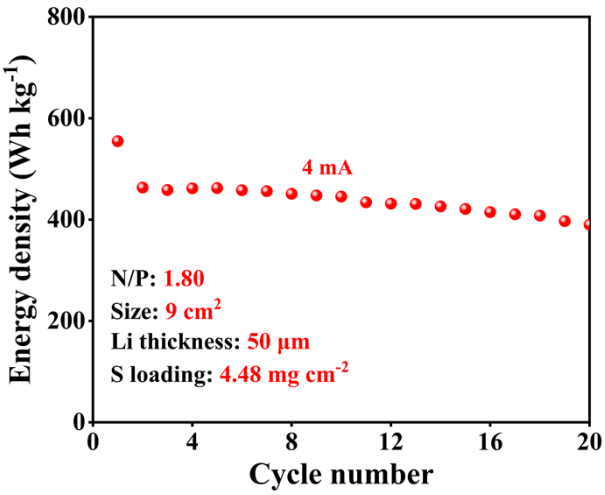

Fig. S28. Gravimetric energy density of the pouch cell under low N/P ratio.

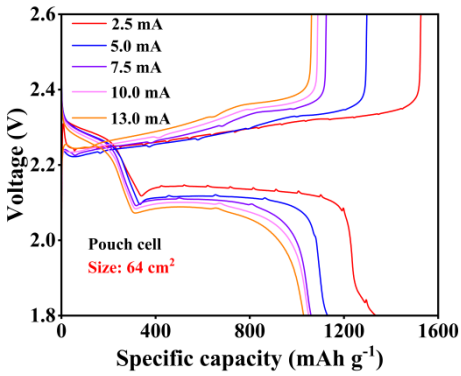

Fig. S29. The rate property of the large-area Li-S pouch cell.

Table S1. Performance metrics of the pouch cell under low N/P ratio.

Cathode		Anode	Separator	Initial areal capacity (mAh cm^{-2})	Initial energy density (Wh kg^{-1})
Carbon paper (mg cm^{-2})	S/C/binder (mg cm^{-2})	Li anode (mg cm^{-2})	LCCO-separator (mg cm^{-2})		
6.99	9.34	2.67	3.72	5.73	554.84
Cell mass: 22.72 mg cm^{-2}					

The gravimetric energy density is calculated based on the weight of the key components, including the current collector, Li anode, cathode coating, and separator. [1]

$$\text{Gravimetric energy density (Wh kg}^{-1}) = \frac{Areal\ capacity\ (mAh\ cm^{-2}) \times 2.2V}{Cell\ mass\ (mg\ cm^{-2})} = \frac{5.73\ (mAh\ cm^{-2}) \times 2.2V}{22.72\ (mg\ cm^{-2})}$$

[1] Z. Z. Chen, M. J. Lu, Y. Qian, Y. Yang, J. Liu, Z. Lin, D. J. Yang, J. Lu, X. Q. Qiu, Ultra-low dosage lignin binder for practical lithium-sulfur batteries, *Adv. Energy Mater.*, 2023, **13**, 2300092.